NACA

RESEARCH MEMORANDUM

SUPERSONIC WAVE INTERFERENCE AFFECTING STABILITY

By Eugene S. Love

Langley Aeronautical Laboratory
Langley Field, Va.

NATIONAL ADVISORY COMMITTEE
FOR AERONAUTICS

WASHINGTON

March 8, 1956

NATIONAL ADVISORY COMMITTEE FOR AERONAUTICS

RESEARCH MEMORANDUM

SUPERSONIC WAVE INTERFERENCE AFFECTING STABILITY

By Eugene S. Love

SUMMARY

Some of the significant interference fields that may affect stability of aircraft at supersonic speeds are briefly summarized. Illustrations and calculations are presented to indicate the importance of interference fields created by wings, bodies, wing-body combinations, jets, and nacelles.

INTRODUCTION

In aircraft and missile configurations one aerodynamic surface more often than not lies within the region of influence of the flow field generated by another aerodynamic surface or by a jet. When this occurs, the flow field is regarded as an interference flow field. This paper will attempt to cover, in a general way, interference flow fields that may affect stability, not with the idea that these fields have not been known to exist, but rather with the intent of drawing increased attention to their relation to stability.

The interference from vortex flows is known to have important effects upon stability; however, vortex flows and viscous effects will, with minor exceptions, be neglected.

SYMBOLS

A	aspect ratio
b	span
c	chord
C_{m_α}	slope of pitching-moment curve
C_{n_β}	rate of change of yawing-moment coefficient with sideslip

C_Y side-force coefficient

D body diameter

d_j jet diameter at jet exit

M_∞ free-stream Mach number

M_j jet Mach number at jet exit

p local static pressure

p_j static pressure at jet exit

p_∞ free-stream static pressure

q local dynamic pressure

q_∞ free-stream dynamic pressure

S surface area

x longitudinal coordinate

y spanwise coordinate

z vertical coordinate

α angle of attack

β sideslip angle; also $\sqrt{M_\infty^2 - 1}$

γ_∞ specific-heat ratio of free stream

γ_j specific-heat ratio of jet

δ flow-deflection angle; also bluntness angle of airfoil

ϵ upwash angle

θ_N nozzle divergence angle

θ_s shock angle

DISCUSSION

Wings

Consideration will be given first to the interference flow fields arising from the wings. Figure 1 presents the portion of a two-dimensional wing interference flow field bounded by the leading-edge and trailing-edge shocks, generally referred to as the direct field of the wing as contrasted with the indirect field, which is defined as the field downstream of the trailing-edge shock. Superposed on the direct field are a body and tail surfaces. Insofar as the tail surfaces only are concerned, the effects of the indirect wing interference field are, in general, not large until the direct field comes in close proximity of the tail surfaces. As illustrated by the direct field, the effect of increasing Mach number is to sweep the field back over the tail surfaces as shown. When this occurs, the properties of the flow field in which the vertical tail yaws and horizontal tail pitches may be significantly altered; as a result, large changes in the tail contribution to stability may be expected. The variation in dynamic pressure in the direct field is indicated at several positions by the ratio of local to free-stream dynamic pressure q/q_∞ and is seen to be appreciable.

Figure 2 shows the direct flow field at $M_\infty = 3.0$ with the configuration at an angle of attack. A comparison of the field with that given in figure 1 for the same semiwedge angle of the leading edge δ and the same thickness ratio t/c shows that the effect of increasing α is to decrease the dynamic pressures in the upper-surface interference field, the converse being true for the lower-surface interference field. Also, increasing α tends to move the direct field off the tail surfaces. In contrast with the effect of angle of attack, when the wing is placed at incidence as might occur with missiles (illustrated in the sketch at the bottom of fig. 2), the direct field from the upper surface moves well onto the upper tail surfaces.

In order to emphasize the effects of angle of attack and to show in proper perspective the effects of bluntness and of thickness on the dynamic pressures in the direct field, figure 2 also shows the configuration with a flat-plate wing $\left(\delta = 0^\circ, \ \frac{t}{c} = 0\right)$. Thickness distribution and thickness ratio alter, for the most part, the distribution of dynamic pressure, whereas the wing bluntness is the primary factor in determining the general magnitude of the dynamic pressures. This effect may be readily visualized at $\alpha = 0^\circ$ by considering the thickness ratio to be reduced by thinning the center portion of the wing while holding the bluntness, or semiwedge angle δ of the wing, constant. Obviously, the Mach number at which this type of interference is encountered is dependent upon overall geometry; for example, the low position of the horizontal tail

indicated in figure 1 at $M_\infty = 3.0$ would be well removed from the trailing shock of the direct field. The present trend in the design of supersonic aircraft is toward much shorter tail lengths than pictured; for such configurations the direct fields would be encountered at lower Mach numbers than implied by these examples. This type of interference diagram can also be of assistance in estimating, for example, where a given amount of vertical tail area might be added to obtain the most favorable gain in yaw stabilization, or in assessing the downwash in the region of tail surfaces immersed in the direct field.

An experimental illustration of the effects of Mach number and angle of attack shown in figures 1 and 2 may be seen in figure 3 which presents schlieren photographs of a configuration of similar geometry in which the two-dimensional portions of the wing flow field are accentuated in the profile views.

In the lower-surface interference flow field for $M_\infty = 3.0$ and $\alpha = 20^\circ$ shown in figure 2, a significant loss in dynamic pressure remains near the downstream edge of the interference field, although the local Mach number is obviously still less than the free-stream value. This loss may be traced directly to the shock losses. Some discussion of the shock losses, or the "q-loss" effects thus seems in order. In figure 4 curves for constant local shock inclination θ_s are presented which show the dynamic-pressure ratio q_1/q_∞ as a function of the free-stream Mach number M_∞ for the particular case of the flow downstream of the shock having returned to a Mach number M_1 that is essentially equal to M_∞; that is, $M_1 = M_\infty$ without being affected by a change in shock inclination. Such conditions occur only in two-dimensional flows, but these flows serve to illustrate the point in simplified form. A two-dimensional surface satisfying these conditions is shown in the upper right of figure 4. In the region immediately downstream of the centered expansion, but upstream of the reflected influence from the shock, the only significant difference of the local flow from the free-stream flow is a loss in dynamic pressure. If a stabilizing surface (as illustrated by the flat plate) were yawed in this region, the side force acting on this surface would be reduced by the factor q_1/q_∞ as compared to that acting on the same surface yawing in the free stream. Therefore, the surface area must be increased by the ratio q_∞/q_1; that is, $S_1 = \frac{q_\infty}{q_1} S_\infty$, if the surface is to realize the same side force that is obtained by the original surface area S_∞ in free stream. For example, at $M_\infty = 3.5$ and $\theta_s = 48^\circ$ ($\delta \approx 30^\circ$) the area of the surface would need to be doubled. Downstream of the initial reflection from the shock the required increase in area would be lessened according to the influence of the attenuation in shock strength.

With regard to shock strength, there is the inherent requirement that, for q-loss effects to be significant, the shock must be strong. Values of the shock-strength parameter ($M_\infty \sin \theta_s - 1$) are superposed on the q-loss curves. Since normal shocks have zero strength at $M_\infty = 1$, it is clear that, in general, the q-loss effect becomes important only at the higher free-stream Mach numbers. The shock-strength parameter affords a simple and convenient means of judging the necessity for considering the possibility of significant q-loss effects.

This simplified illustration of the q-loss effect indicates that conditions will arise where it will be necessary to account for, or compensate for, this effect upon stabilizing surfaces by increasing stabilizing-surface area, improving the lift effectiveness of the surface, or by juggling the q-loss through changes in configuration design. For realistic configurations such as those shown in the lower right of figure 4, the determination of the q-loss and the necessary compensation requires more elaborate calculations. However, it may be reasoned that at the higher Mach numbers a blunt-nose configuration having a detached shock may produce a large q-loss and a large gradient in q-loss; canard surfaces placed well forward would be subjected to these losses. A typical supersonic aircraft configuration as illustrated might experience significant q-loss effects upon its tail surfaces as a result of the total loss through shocks from the nose, canopy, and wing leading and trailing edges, although the individual shocks might have relatively small q-loss effects. In recent tests of a configuration having a short fuselage, the vortex layer stemming from the intersection of the nose and canopy shocks was observed to pass across the vertical tail. Since this vortex layer divides regions of different q-loss, this phenomenon may prove to be another factor for consideration. For configurations at high angle of attack, the q-loss and also the q-gain (such as shown previously for the lower surface of wings at angle of attack) may be expected to have important effects.

Beyond Mach numbers of the order of about 1.3, the downwash that exists at the trailing edge of an airfoil at lower speeds reverts to upwash. This upwash is considered in figures 5 and 6 for two-dimensional airfoils and fields of flow. The magnitude of the initial upwash ϵ_i immediately downstream of the trailing edge of a symmetrical airfoil is shown in figure 5. The initial upwash increases with Mach number, angle of attack, and bluntness; at the higher Mach numbers and angles of attack, it is apparent that the initial upwash of even a flat plate cannot be considered negligible.

The upwash that is likely to occur in the vicinity of a downstream horizontal tail as a result of the presence of the wing is of particular importance. In this regard, the relative magnitude of the initial upwash for the flat plate and blunt airfoil may be misleading and must be moderated because of the manner in which the downstream interference from

the wing flow fields reduces the upwash. At the top of figure 6 the downstream upwash for a flat plate is illustrated. As shown by the sketch, the initial upwash from the trailing edge of the flat plate does not decrease until some distance x_i is reached, at which point the wing interference field begins to reduce the upwash. An example of the variation of x_i/c with Mach number is shown to the right of the sketch. The effect that increasing Mach number has in increasing the initial upwash, as was shown in figure 5, is seen to be offset by the decrease in the downstream extent of the initial upwash. It is important to note, however, that at $M_\infty = 5$ the initial upwash angle, which is about 4° for this angle of attack, would remain for about a half chord length downstream before it would begin to decrease.

For the thick airfoil the initial upwash begins to decrease immediately behind the trailing edge since the wing interference field comes into play immediately, as shown by the sketch in the lower portion of figure 6. An example of the decay in upwash for a thick airfoil is shown to the right of the sketch. From this example, one may conclude that at large α and high Mach numbers, tail surfaces that are closely coupled to the wings will experience several degrees of upwash. Further, the large upwash near the trailing edge of the wing is important to wing-body interference.

Bodies

The interference flow fields created by bodies will be considered next. Figure 7 presents isobar-streamline fields for a slender and a bluff body. (The field for the slender body was obtained by extensions to the characteristic calculations of ref. 1.) For clarity only a few of the calculated isobars and streamlines are shown for the bodies. It is apparent that the aerodynamic characteristics of surfaces immersed in such fields will be altered considerably, as will be shown subsequently. The field for the bluff body is quite different from that for the slender body. In the bluff-body field the division line of pressure gradients that has its orgin at the point of tangency on the body surface is sharply defined. Ahead of this line the pressures in the field are falling; behind it they are rising.

Inasmuch as the nose shock establishes the forward limit of the body interference field, it is of interest to examine the forward limit of the field as given by the exact shock and by the commonly employed approximate limits given by the shock based on the nose angle only and by the free-stream Mach line. Figure 8 presents a comparison of the exact and the approximate limits at several Mach numbers for the bluff body of the preceding figure. One readily observes that large errors may be introduced by either of the approximate limits. An example of the reliability of the

exact shock calculations may be seen by comparing the calculated exact shock for $M_\infty = 1.94$ with the upper left-hand schlieren photograph of figure 3. The wing and forebody are the same for both the calculation and the photograph; the experimental nose shock is seen to touch the forward wing tip as predicted by the exact calculation. Figure 8 also shows that the division line of pressure gradients experiences significant changes in inclination with Mach number.

As an aid in illustrating the effect of flow inclinations produced by the body, the flow inclination has been calculated at several Mach numbers for the point in the field designated in figure 8 by the circled cross $\left(\frac{x}{D} = 4.18, \quad \frac{y}{D} = 2.50\right)$. In the upper left of figure 9 the calculated inclination at this point is presented as a function of Mach number. In general, the flow inclination increases with free-stream Mach number until the exact shock passes behind the point at $M_\infty \approx 2.63$. This change of flow inclination with Mach number explains for the most part some results of a skewed-store investigation conducted at the Langley Laboratory (ref. 2). These results at Mach numbers of 1.41 and 1.96 are shown in the lower half of figure 9. The side-force coefficient of the store in the presence of the wing-body combination is shown for the skewed and unskewed condition. The order of magnitude of the skew necessary to produce zero side force at $\alpha = 0^\circ$ is in general agreement with that indicated to be necessary from a consideration of the flow inclination created by the body alone (upper left). Some differences are to be expected because of the omission of the effects of the presence of the wing and because of differences in body geometry. The experimental store investigation of reference 2 also showed that increasing the forebody length (no change in forebody shape) reduced the amount of skew necessary for $C_Y = 0$ at $\alpha = 0^\circ$. This variation is also to be expected as indicated by the calculated change in flow inclination with forebody length shown in the upper right of figure 9.

Wing-Body Interference

The interference between bodies and wings is considered in this section. Wing-body interference has been and remains the subject of extensive theoretical and experimental studies and is perhaps the most familiar type of interference problem. Therefore, only a few aspects of the problem are considered herein. It is instructive to examine first a general representation of wing-body interference. Figure 10 presents some examples of experimental results in the low angle-of-attack range from tests at the Langley Laboratory (refs. 3, 4, and 5) of wing-body combinations which show, in additive form, the ratio of the slope of the pitching-moment curve of the components and of the interference quantities to the slope of the pitching-moment curve of the wing-body combination where:

W_e	exposed wing alone
W(B)	wing in presence of body
w(b)	interference on wing due to body
B	body alone
b(w)	interference on body due to wing
WB	wing-body combination
C_{m_α}	slope of pitching-moment curve

For emphasis, the regions corresponding to interference quantities have been cross-hatched, single cross-hatching denoting a positive moment contribution and double cross-hatching meaning a negative moment contribution.

For most aircraft configurations that are subjected to significant interference at low angle of attack, the interference on the body due to the wing b(w) is more important than the interference on the wing due to the body w(b), as indicated in these examples. Particular attention is drawn to the interference on the body due to the wing and to its variation with the ratio of wing span to maximum body diameter b/D. Since this interference is always stabilizing it is apparent that the wing-lift carryover effects upon the body are more important than the tip effects which are destabilizing. As b/D increases, both the wing-lift carryover effects and tip effects move rearward on the body, and eventually the tip effects move off the body. At a value of b/D corresponding to the condition for which tip effects would vanish (as illustrated by the sketches) the interference on the body due to the wing reaches a maximum; further increase in b/D reduces the interference as the result of loss of wing-lift carryover.

The relation of the wing interference field to this interference on the body due to the wing is illustrated in figure 11 for a series of rectangular wing and body combinations for which the chord of the wing was held constant. The upper portion of the figure presents only the interference on the body due to the wing (in the same form as shown in fig. 10) as a function of b/D for several Mach numbers, and as a function of Mach number for several values of aspect ratio A (and span-diameter ratio). The point to be noted is not so much the similar areas represented by the interference quantities, whether expressed as a function of b/D or of M_∞, which may result from no more than a fortuitous choice of scales of the abscissas, but rather the similar trends in the interference pitching moment with either b/D or M_∞. Because of these similar trends, it is suspected that the results may be correlated on the

basis of equal areas of influence created on the body by the wing. On this basis a simple expression may be derived that will give equal areas of influence on the body from a strip on the wing for rectangular wing and cylindrical body combinations. This expression is $M_i \approx \left(\frac{A^2}{2\beta}\right)\left(\frac{D}{b}\right)c^3 p_i$ where M_i is the interference pitching moment, p_i is the average interference pressure, and β is the speed parameter $\sqrt{M_\infty^2 - 1}$. Inasmuch as the chord is constant for the wings of this series, the results may be correlated by the factor $\left(\frac{A^2}{2\beta}\right)\left(\frac{D}{b}\right)$ with the implication that differences observed in such a correlation are indicative of the changes in p_i due to Mach number. The correlation is shown at the bottom right and serves to substantiate the idea that the observed similarities in trends of the interference pitching moment are due primarily to simulation of equivalent areas of influence.

Figure 12 presents schlieren photographs illustrating a type of interference that stems from wing-body junctures and is apparently peculiar to lifting conditions. The top two photographs at $M_\infty = 2.62$ show that under lifting conditions a shock may originate near the trailing edge of the wing at the wing-body juncture as the result of wing-body interaction and viscous effects. Shocks of this type can interact with the horizontal tail and affect the longitudinal stability. With decreasing Mach numbers such shocks tend to become more diffuse, as shown at $M_\infty = 2.22$; at $M_\infty = 1.62$ separation occurs ahead of the wing-root juncture, and the shocks and downstream pressure gradients associated with this separation alter the loading on the wing.

Jets and Nacelles

The theoretical interference flow field produced by a supersonic jet exhausting into a supersonic stream is illustrated in figure 13 in isobar-streamline form. (The basic characteristic net for fig. 13 is given in ref. 1; the isobars were computed from this net.) The initial conditions are indicated in the figure. The static-pressure ratio of about 9 corresponds to the upper limit of operation of turbojet with afterburner or to the lower or moderate range of rocket operation. Attention is directed to the large gradients in pressure and to the flow inclinations that occur in the ambient field as a result of the jet's presence. Of particular importance in evaluating the limits of the interference field is the large curvature of the exit shock. This curvature is accentuated for jet interference fields by the transition from a two-dimensional turning at the jet exit to a three-dimensional turning away from the jet exit.

Figure 14 gives some examples of the calculated pressures that the interference field of figure 13 would create on a flat plate immersed in the field at several radial positions. Only the pressure immediately downstream of the interaction of the exit shock with the plate are presented. It is at once apparent that the jet may create large loads on the plate and that the regions of influence may be extensive. The importance of the plate position in the field and its angle of attack are equally apparent. These theoretical indications are in qualitative agreement with experimental findings. (See ref. 6, for example.)

If the plate considered in figure 14 were a stabilizing surface, the jet would be expected to have a significant effect upon stability. At the top of figure 15 the calculated jet and interference field has been reproduced to scale in conjunction with a supersonic aircraft configuration. For an inboard nacelle location as shown, the jet interference field would interact with both the vertical and horizontal tail surfaces. For an outboard location there would be less need for considering the jet-interference field, but the nacelle-interference field would have a direct effect. An experimental example of nacelle interference obtained in tests at the Ames Laboratory is shown at the bottom of the figure. The lateral stability derivative C_{n_β} is presented as a function of Mach number for the configuration shown on the right with nacelles off and for the complete configuration. At low Mach numbers the nacelle interference produces a significant loss in C_{n_β}, whereas at the higher Mach numbers, where the nacelle nose shock interacts with the vertical tail, this loss is reduced.

CONCLUDING REMARKS

A summary has been presented of some of the more important interference fields that may affect stability at supersonic speeds. Illustrations and calculations are included to show the importance of interference fields created by wings, bodies, wing-body combinations, jets, and nacelles.

Langley Aeronautical Laboratory,
National Advisory Committee for Aeronautics,
Langley Field, Va., November 2, 1955.

REFERENCES

1. Schäfer, M.: Steady Supersonic Flows. British M.A.P. Völkenrode. Reps. and Translations No. 995, Apr. 15, 1948. Reps. and Translations No. 996, May 1, 1948.

2. Guy, Lawrence D.: Loads and External Stores at Transonic and Supersonic Speeds. NACA RM L55E13b, 1955.

3. Coletti, Donald E.: Investigation of Interference Lift, Drag, and Pitching Moment of a Series of Triangular Wing and Body Combinations at a Mach Number of 1.94. NACA RM L55I14, 1955.

4. Coletti, Donald E.: Investigation of Interference Lift, Drag, and Pitching Moment of a Series of Triangular Wing and Body Combinations at a Mach Number of 1.62. NACA RM L55B25, 1955.

5. Coletti, Donald E.: Investigation of Interference Lift, Drag, and Pitching Moment of a Series of Rectangular Wing and Body Combinations at Mach Numbers of 1.62, 1.93, and 2.41. NACA RM L52E26, 1952.

6. Bressette, Walter E.: Investigation of the Jet Effects on a Flat Surface Downstream of the Exit of a Simulated Turbojet Nacelle at a Free-Stream Mach Number of 2.02. NACA RM L54E05a, 1954.

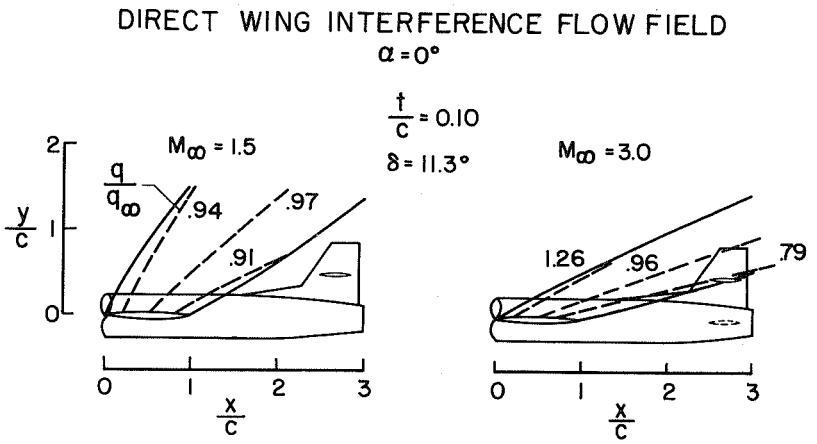

Figure 1

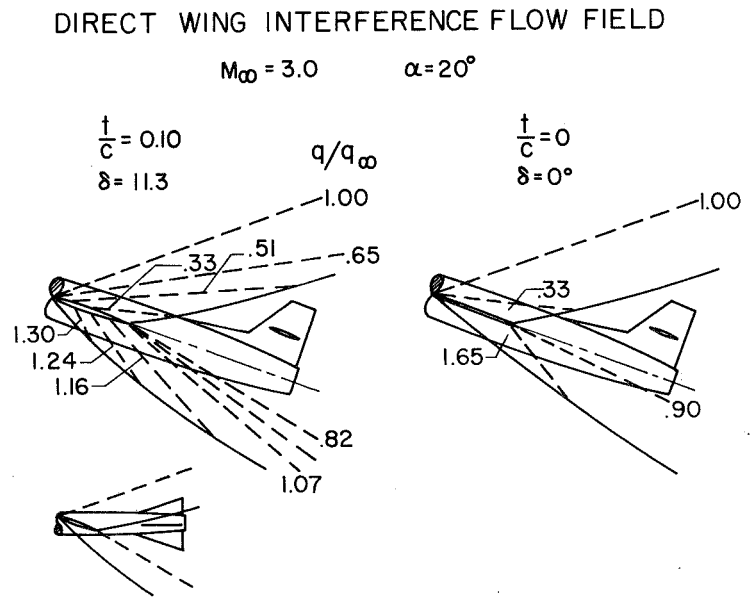

Figure 2

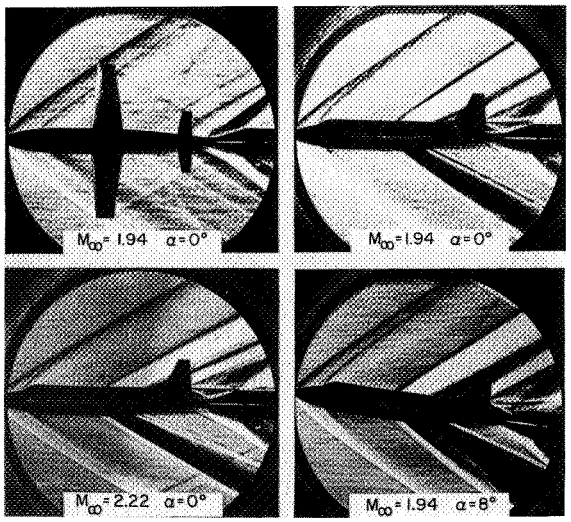

L-91764

Figure 3

"q-LOSS" EFFECT

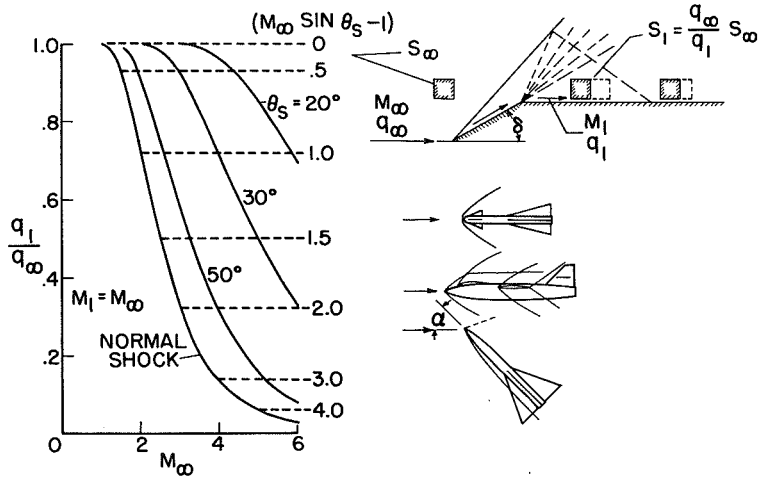

Figure 4

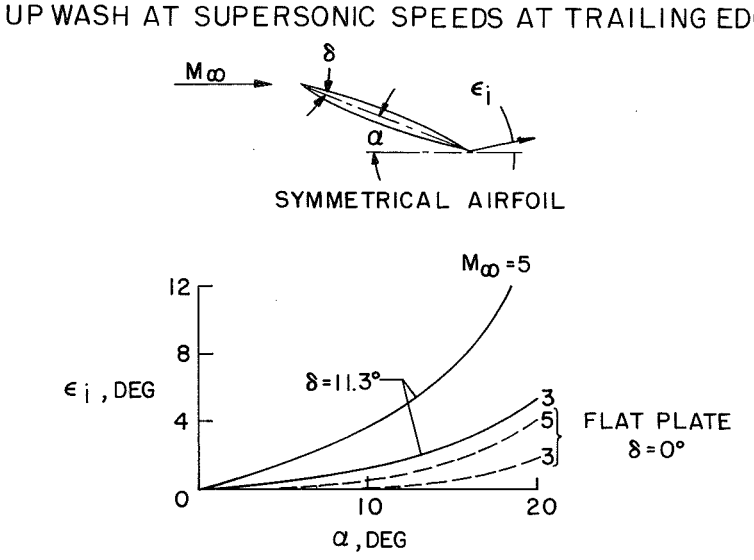

Figure 5

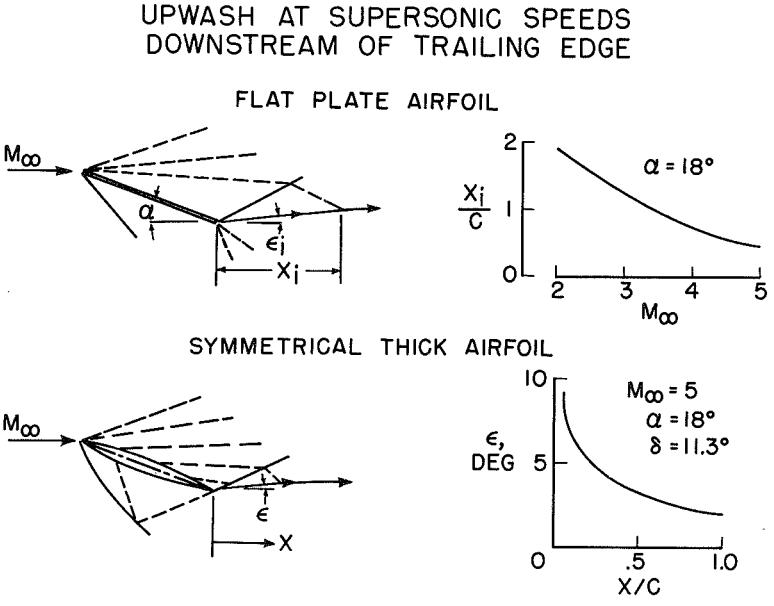

Figure 6

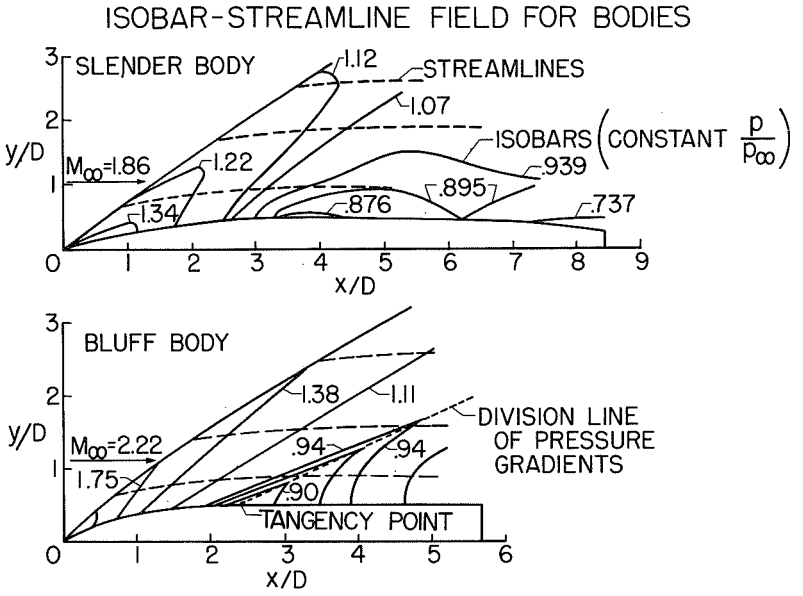

Figure 7

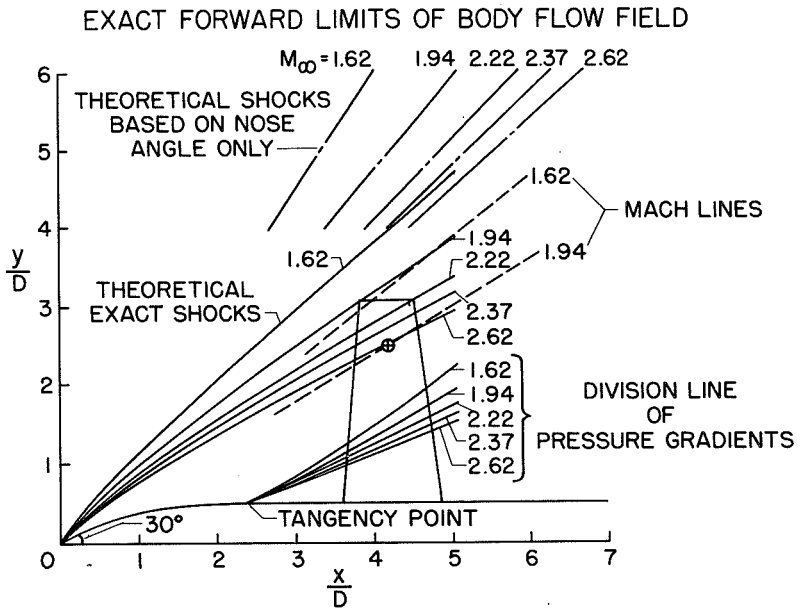

Figure 8

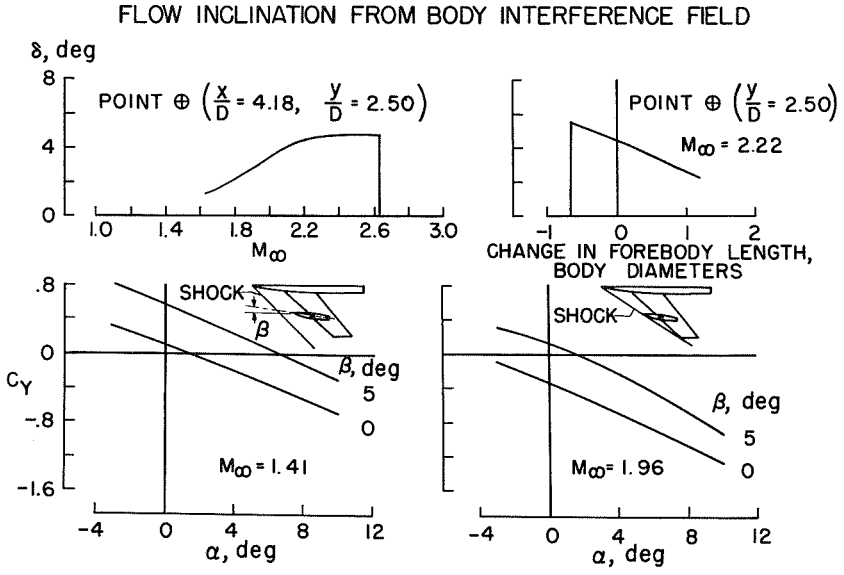

Figure 9

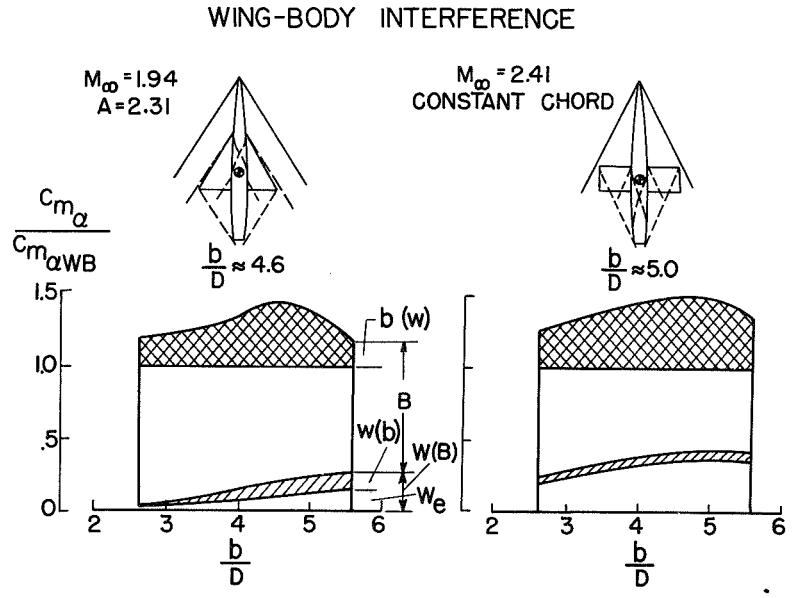

Figure 10

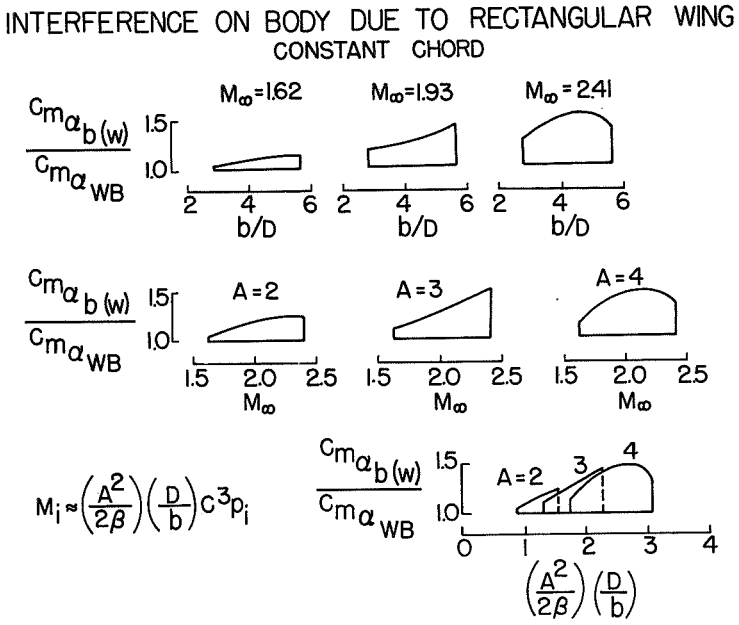

Figure 11

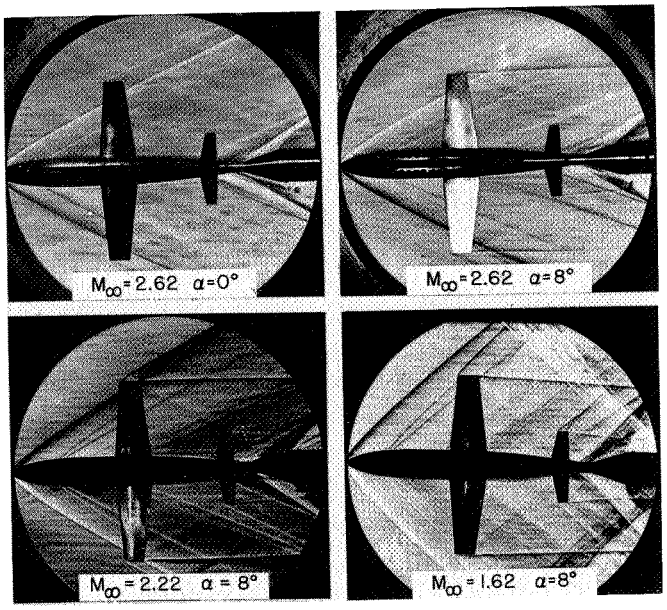

L-91765

Figure 12

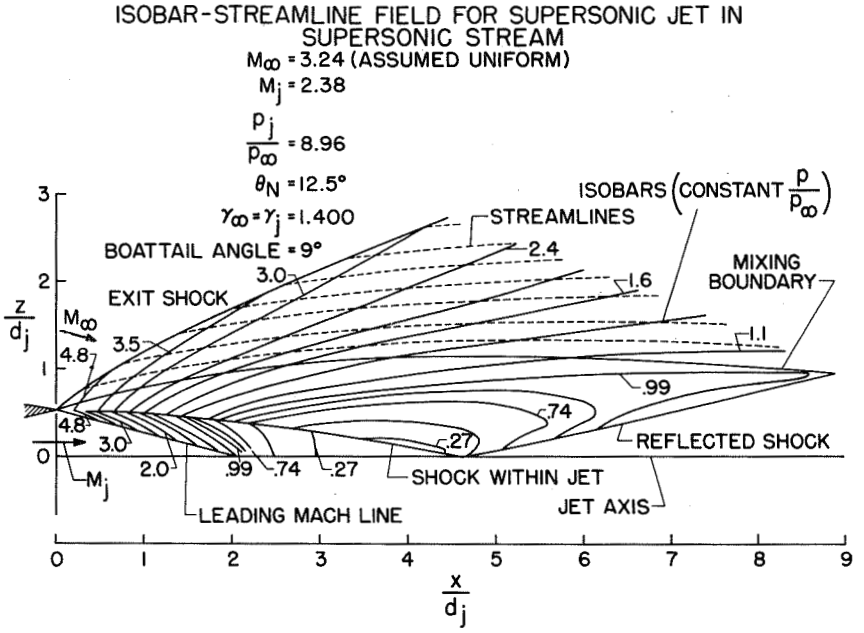

Figure 13

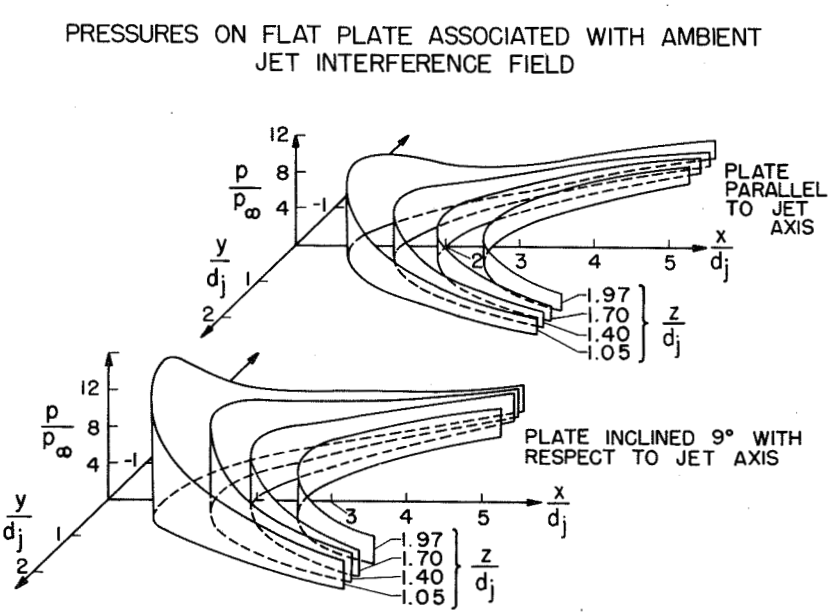

Figure 14

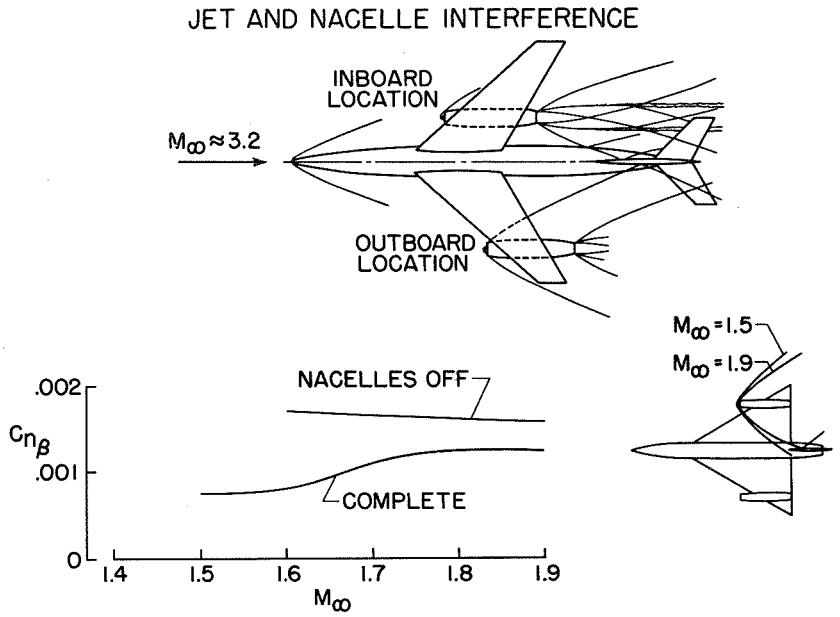

Figure 15

NACA - Langley Field, Va.